Inorganic Chemistry

Article

pubs.acs.org/IC

Coordination-Driven Self-Assembly of a 2D Graphite-Like Framework Constructed from High-Nuclear Ce_{10} Cluster Encapsulated Polyoxotungstates

Pengtao Ma, Rong Wan, Yueyan Wang, Feng Hu, Dongdi Zhang, Jingyang Niu,* and Jingping Wang*

Henan Key Laboratory of Polyoxometalate Chemistry, Institute of Molecular and Crystal Engineering, College of Chemistry and Chemical Engineering, Henan University, Kaifeng, Henan 475004 P. R. China

Supporting Information

ABSTRACT: It is challenging to explore and prepare high-nuclear lanthanide (Ln) cluster-encapsulated polyoxometalates (POMs). Herein, we fabricate an unprecedented Ce_{10}-cluster-embedded polyoxotungstate (POT) $(TMA)_{14}H_2[Ce^{III}(H_2O)_6]\{[Ce^{IV}_7Ce^{III}_3O_6(OH)_6(CO_3)(H_2O)_{11}][(P_2W_{16}O_{59})]_3\}\cdot 41H_2O$ (**1**) (TMA = tetramethyleneamine) by coordination-driven self-assembly strategy, which contains the largest Ce cluster $[Ce^{IV}_7Ce^{III}_3O_6(OH)_6(CO_3)(H_2O)_{11}]$ (Ce_{10}) in all the Ln-containing POM chemistry to date. Self-assembly of the in situ dilacunary $[P_2W_{16}O_{59}]^{12-}$ fragments and mixed Ce^{3+} and Ce^{4+} ions by means of coordination-driven force results in a novel 2D graphite-like framework constructed from mixed-valent cerium(III/IV) cluster $\{Ce_{10}\}$ encapsulated poly(POT) units and Ce^{3+} ions. The most remarkable feature is that the skeleton of the centrosymmetric Ce_{10}-cluster-embedded POT trimer contains three dilacunary $[P_2W_{16}O_{59}]^{12-}$ fragments trapping a novel $\{Ce_{10}\}$ cluster via 18 terminal-oxo and three μ_4-oxo atoms.

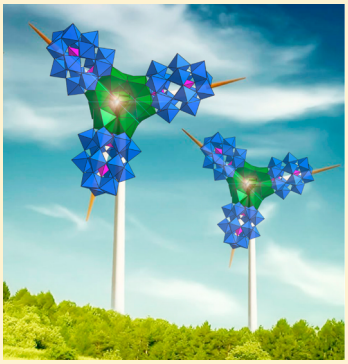

INSTRUCTION

Metal−organic frameworks (MOFs) materials are a large family of well-known hybrid solids with infinite networks built from organic bridges and inorganic nodes, which renders them to have many potentials in diverse areas such as catalysis, ion exchange, separation, gas adsorption and storage, etc.[1] In contrast, cluster based frameworks (CBFs) with metal clusters as connecting nodes and organic groups, metal ions or their complexes as bridges, are a novel type of solid materials, which can make CBFs bear desirable combining properties of clusters and MOFs. Utilizing large cluster building units (CBUs) as nodes to construct unique CBFs is particularly interesting. To date, the usual CBUs in the construction of CBFs mainly are small metal carboxylate clusters.[2]

It is well-known that polyoxometalates (POMs) are attractive inorganic building blocks, which have the excellent capability to bind transition-metal (TM) or lanthanide (Ln) centers, and bear their inherent physical and chemical properties of bifunctional components, have been evidenced as diverse robust molecular species displaying novel conductive, magnetic, luminescence, and catalytic or photocatalytic properties.[3] Therefore, POMs can be employed as CBUs for the construction of CBFs, which might merge POM's merits to generate extra-large nanosized holes or channels with special properties. Until now, the study of CBFs is still in its infancy, and the CBFs constructed by POM-based aggregates encapsulating high-nuclear TM or Ln clusters have been rarely found,[4] although great progress has been made for POM-based MOF materials in recent years.[5] In the domain of POM chemistry, high-nuclear TM cluster incorporated polyoxotungstates (HTMCIPs) have been extensively explored, and some impressive examples such as the Mn_{19},[6] Cu_{20},[7] Fe_{28},[8] Ni_{20},[9] and Zr_{24}[10] HTMCIPs have been already reported; however, it is difficult from them to generate CBFs thanks to the lack of effective connectors linking these HTMCIP CBUs together. On the contrary, Ln centers with high coordination requirements and oxophile capacity can serve as linkers to integrate polyoxotungstate (POT) subunits into giant poly(POTs) or multidimensional frameworks, in general, which are not apt to aggregate Ln centers into Ln clusters in POM system. Therefore, the research on the chemistry of high-nuclear Ln comprising POTs remains underdeveloped, albeit only a handful of examples with eight or more Ln centers have been made such as $[Ce_{20}Ge_{10}W_{100}O_{376}(OH)_4(H_2O)_{30}]^{56-}$,[11] $[Ce_{16}As_{12}W_{148}O_{524}(H_2O)_{36}]^{76-}$,[12] $[Cs\subset Ln_6As_6W_{63}O_{218}(H_2O)_{14}(OH)_4]^{25-}$ (Ln = Eu^{3+}, Gd^{3+}, Tb^{3+}, Dy^{3+}, Ho^{3+}, Er^{3+}),[13] $[Ln_{16}As_{16}W_{164}O_{576}(OH)_8(H_2O)_{42}]^{80-}$ (Ln = Eu^{3+}, Gd^{3+}, Tb^{3+}, Ho^{3+}),[14] $[Gd_8As_{12}W_{124}O_{432}(H_2O)_{22}]^{60-}$,[15] $[Yb_{10}As_{10}W_{88}O_{308}(OH)_8(H_2O)_{28}(OAc)_4]^{40-}$,[16] and $[Tb_8(pic)_6(H_2O)_{22}(B\text{-}\beta\text{-}AsW_8O_{30})_4(WO_2(pic))_6]^{12-}$.[17] It should be pointed out that the Ln centers in these high-nuclear Ln-substituted POTs prevailingly exist individually and serve as linkers; the reports on high-nuclear Ln cluster incorporated POTs (HLCIPs) are sporadic, and only one Ln_6-cluster POT of $[\{Yb_6(\mu_6\text{-}O)(\mu_3\text{-}OH)_6(H_2O)_6\}(\alpha\text{-}P_2W_{15}O_{56})_2]^{14-}$ has been addressed hitherto.[18] Can much higher nuclear Ln clusters be incorporated to POTs? Can the resulting HLCIPs function as

Received: October 26, 2015
Published: January 5, 2016

DOI: 10.1021/acs.inorgchem.5b02473
Inorg. Chem. 2016, 55, 918−924

CBUs and be further assembled to the CBFs by taking advantage of coordination-driven effect of Ln connectors? This is a challenging topic, which provokes our keen interest and provides us a great opportunity.

In the search for high-nuclear Ln coordination complexes featuring Ln_nO_m cores, we found that cerium oxide cores can create various highly condensed derivatives including {Ce_6}, {Ce_{10}}, {Ce_{22}}, etc.[19] Inspired by these enlightening results, we began to focus on constructing novel functional CBFs based on HLCIP CBUs through coordination-driven effect of Ln ions. Thus, the trivacant $[P_2W_{15}O_{56}]^{12-}$ precursor was selected to react with Ce^{3+} salts under the protection of isonicotinic acid; finally, an unprecedented CBF on the base of Ce_{10} CBUs $(TMA)_{14}H_2[Ce^{III}(H_2O)_6]\{[Ce^{IV}{}_7Ce^{III}{}_3O_6(OH)_6(CO_3)(H_2O)_{11}][(P_2W_{16}O_{59})]_3\}\cdot 41H_2O$ (**1**) was successfully made, in which an unseen mixed-valent {Ce_{10}} cluster was trapped by three in situ formed dilacunary fragments $[P_2W_{16}O_{59}]^{12-}$. More intriguingly, the novel two-dimensional (2D) graphite-like CBF is constructed from mixed-valent (III/IV) {Ce_{10}} cluster encapsulated POTs through peripheral Ce^{3+} ions. **1** not only represents the largest HLCIP but also is the first graphite-like CBF assembled from HLCIP CBUs to date. This finding opens the avenue for profoundly exploring HLCIP-based CBFs and further exploiting their functional applications; as a result, the creativity and significance of this work are undoubted.

EXPERIMENTAL SECTION

Materials and Methods. $Na_{12}[P_2W_{15}O_{56}]\cdot 24H_2O$ was prepared according to the reference[20] and confirmed by IR spectrum. Other chemical reagents were purchased and used without further purification. IR spectra were recorded on a Bruker VERTEX 70 IR spectrometer using KBr pellets in the range of 4000−400 cm^{-1}. Powder XRD patterns were obtained using a Bruker D8 ADVANCE diffractometer with Cu Kα radiation (λ = 1.540 56 Å). Variable-temperature magnetic susceptibility data were obtained on a SQUID magnetometer (Quantum Design, MPMS3) in the temperature range of 1.8−300 K. Thermogravimetry analyses (TGA) were performed on a NETZSCH STA 449 F5 Jupiter thermal analyzer in flowing N_2 with a slow heating rate of 5 °C min^{-1}. ^{31}P NMR spectra were detected in 5 mm tubes with ^1H decoupling on a Bruker AV-400 model spectrometer operating at 400 MHz. ^{31}P chemical shifts were referenced to the 85% H_3PO_4 as external standard. Elemental analyses of C, H, and N were performed with a PerkinElmer 2400−II CHNS/O analyzer. Energy-dispersive X-ray spectroscopy (EDX) measurement was performed on a JSM-7610F scaning electron microscope using OXFORD x-act EDX.

Preparation of $(TMA)_{14}H_2[Ce^{III}(H_2O)_6]\{[Ce^{IV}{}_7Ce^{III}{}_3O_6(OH)_6(CO_3)(H_2O)_{11}][(P_2W_{16}O_{59})]_3\}\cdot 41H_2O$ (1). $CeCl_3\cdot 7H_2O$ (0.075 g, 0.200 mmol) was dissolved in 20 mL of H_2O, then solid isonicotinic acid (0.074 g, 0.600 mmol) was added, and the mixture was stirred until the solid was completely dissolved. The pH of the resulting solution was adjusted to 4.5 by using 6 mol·L^{-1} NaOH, and the solution continued to stir for 10 min at room temperature. Then solid $Na_{12}[P_2W_{15}O_{56}]\cdot 24H_2O$ (0.440 g, 0.100 mmol) and trace Na_2CO_3 (0.002 g, 0.019 mmol) were added; immediately, the primrose yellow turbid solution was formed. After the pH of the mixture was set at 7.8 with 6 mol·L^{-1} NaOH, it was left stirring at 60 °C for 1 h. Ultimately, the solution turned to be clear and orange, followed by addition of 0.110 g (1.004 mmol) tetramethylammonium chloride under stirring, while the solution was still hot. The resulting solution was filtered and left to slowly evaporate at room temperature, and small yellow crystals of **1** were obtained after approximately one week. Yield: 0.14 g (48% based on $CeCl_3\cdot 6H_2O$). Elemental analysis (%) calcd for **1**: C, 4.35; H, 1.87; N, 1.25. Found: C, 4.34; H, 2.06; N, 1.26. Selected IR (KBr, cm^{-1}): 3419, 3034, 1625, 1484, 1448, 1414, 1090, 1054, 952, 908, 821, 744.

X-ray Crystallography. A single crystal of **1** was sealed in a capillary tube since the crystal is easily efflorescent. Intensity data collection were performed on a Bruker APEX II CCD diffractometer with graphite-monochromated Mo Kα radiation (λ = 0.71073 Å) with an optical fiber as the collimator. Data reduction was accomplished using *SAINT* program,[21] and then the substantial redundancy in data allowed a multiscan absorption correction (SADABS)[22] to be applied, on the basis of multiple measurements of equivalent reflections. The structure was solved by direct methods, developed by successive difference Fourier syntheses, and refined by full-matrix least-squares on all F^2 data using the SHELX program suite.[23] In the final refinement, the W, P, and Ce atoms were refined anisotropically; the O, C, and N atoms were refined isotropically. The partial TMA cations and lattice water molecules were located by Fourier map; the remaining TMA cations and lattice water molecules were determined by CHN element analysis and TGA results. The hydrogen atoms of the TMA groups were placed in calculated positions and then refined using a riding model. All H atoms on water molecules were directly included in the molecular formula. Crystallographic data for the structure reported in this paper have been deposited in the Cambridge Crystallographic Data Center with CCDC Number: 1430500 for **1**. Crystal data and structure refinement parameters are listed in Table 1.

Table 1. Crystal Data and Structure Refinements for 1

empirical formula	$C_{57}H_{292}N_{14}O_{250}P_6Ce_{11}W_{48}$
M	15 726.31
λ (Å)	0.710 73
T (K)	296(2)
cryst syst	orthorhombic
space group	*Pnma*
a (Å)	28.2062(10)
b(Å)	31.0697(11)
c (Å)	40.1622(14)
V (Å)	35 196(2)
Z	4
D_c (g cm^{-3})	2.771
μ (mm^{-1})	17.105
F(000)	25 644
2θ range (deg)	2.49−50
index ranges	$-33 \le h \le 26$, $-36 \le k \le 36$, $-47 \le l \le 41$
measd reflns	178 982
ind reflns	31 610 [R_{int} = 0.0971]
data/restraints/params	31 610/60/831
GOF on F^2	1.083
R indexes [$I \ge 2\sigma(I)$]	R_1 = 0.0590, wR_2 = 0.1360
R indexes [all data]	R_1 = 0.1114, wR_2 = 0.1694

Proton Conductivity Measurements. The powder for alternating-current (AC) impedance measurements was prepared by grinding the sample into a homogeneous powder with a mortar and pestle. The powdered crystalline sample of **1** was compressed to 1.0−1.2 mm in thickness and 12.0 mm in diameter under a pressure of 12−14 MPa. The AC impedance spectroscopy measurement was performed on a chi660d (Shanghai chenhua) electrochemical impedance analyzer with copper electrodes (the purity of Cu is more than 99.8%) over the frequency range from 1×10^5 to 1 Hz. Measurements were taken in the temperature range of 30−100 °C with 98% relative humidity (controlled by using an HDHWHS-50 incubator). ZSimpWin software was used to extrapolate impedance data results by means of an equivalent circuit simulation to complete the Nyquist plot and obtain the resistance values. Conductivity was calculated using the following equation: $\sigma = L/RS$ (**S1**), where L and S are the thickness (cm) and cross-sectional area (cm^2) of the pellet, respectively, and R, which was extracted directly from the impedance plots, is the bulk resistance of the sample, and σ is the conductivity (S cm^{-1}). The equation which is used for estimating to the corresponding activation energy (E_a) of **1** is

DOI: 10.1021/acs.inorgchem.5b02473
Inorg. Chem. 2016, 55, 918−924

listed below. $\sigma T = \sigma_0 \times \exp(-E_a/k_B T)$ (**S2**), where σ is the ionic conductivity, σ_0 is the pre-exponential factor, E_a is the activation energy of the conductivity, k_B denotes the Boltzmann constant, and T is the temperature.

RESULTS AND DISCUSSION

Description of the Structures. X-ray analysis reveals that **1** is a novel 2D CBF based on high-nuclear $\{Ce_{10}\}$ cluster embedded poly(POT) units $\{[Ce^{IV}_7Ce^{III}_3O_6(OH)_6(CO_3)(H_2O)_{11}]\text{-}[(P_2W_{16}O_{59})]_3\}^{19-}$ (**1a**) and $[Ce^{III}(H_2O)_6]^{3+}$ bridges. As shown in Figure 1, **1a** consists of three $[P_2W_{16}O_{59}]^{12-}$ ($\{P_2W_{16}\}$) moieties linked by a $[Ce^{IV}_7Ce^{III}_3O_6(OH)_6(CO_3)(H_2O)_{11}]$ ($\{Ce_{10}\}$) cluster through Ce−O−W and Ce−O−P linkages, leading to a tripod-like trimeric structure with idealized C_{3v} symmetry.

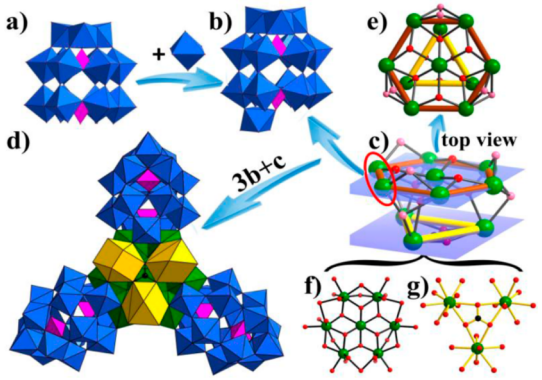

Figure 1. Structures of (a) the precursor $[P_2W_{15}O_{56}]^{12-}$; (b) the $[P_2W_{16}O_{59}]^{12-}$ subunit; (c, e) the $\{Ce_{10}\}$ cluster; (d) the high-nuclearity $\{Ce_{10}\}$ cluster embedded poly(POT) ion $\{[Ce^{IV}_7Ce^{III}_3O_6(OH)_6(CO_3)(H_2O)_{11}]\text{-}[(P_2W_{16}O_{59})]_3\}^{19-}$; (f) the segment ($\{Ce_6(Ce)\}$); (g) the segment $\{Ce_3\}$. Color code for (d): C, black; PO_4 tetrahedral purple; WO_6 octahedral sky bule; green polyhedra Ce^{IV}; and orange polyhedra Ce^{III}.

The $\{P_2W_{16}\}$ moiety (Figure 1b) can be seen as a dilacunary Dawson unit derived from the saturated Dawson-type $\{P_2W_{18}O_{62}\}$ unit. As far as we know, there are two kinds of rare $\{P_2W_{16}\}$-based works in previously literatures up to now. One is derived from removing two edge-shared $\{WO_6\}$ groups at the one polar position of the $\{P_2W_{18}O_{62}\}$ unit (Figure 1b and Scheme S1);[24,25] the other can be formed via the removal of two adjacent $\{WO_6\}$ octahedra from the "belt" region of its parent Dawson-type structure $\{P_2W_{18}\}$ (Scheme S2).[26] The $\{P_2W_{16}\}$ unit is formed from the dissociation and reassembly of the trivacant $[P_2W_{15}O_{56}]^{12-}$ precursor (Figure 1a) during the course of reaction. The $\{Ce_{10}\}$ cluster (Figure 1c,e and Figure S1) can be viewed as a hemispherical architecture, which can formally be devided into two layer-like arrangement: the bottom can be described as a domed hexagonal $\{Ce^{IV}_6(Ce^{IV})O_6(OH)_6(H_2O)\}$($\{Ce_6(Ce)\}$ segment, Figure 1f) reminiscent of the analogous familiar Anderson-type $\{X(OH)_6Mo_6O_{24}\}$ anion,[27] on the top, one triangular $\{Ce^{III}_3(CO_3)(H_2O)_{10}\}$ group ($\{Ce_3\}$, Figure 1g) capps on the $\{Ce_6(Ce)\}$ hexagon. Alternatively, the $\{Ce_{10}\}$ core can be visualized as a similar trivacant Keggin skeleton, in which a seven-coordinated Ce4 central atom merges three $\{Ce_3\}$ triads together via three corner-sharing μ_4-O atoms. To the best of our knowledge, this Ln-oxo cluster showing a similar trivacant Keggin POM skeleton is observed for the first time. This skeleton is obviously different from previously reported $\{Ce_{10}\}$ cluster, where both $\{Ce_2(\mu\text{-}O)_2\}$ and $\{Ce_2(\mu\text{-}O)\}$ groups are attached side-on to the body-centered pentagonal {Ce5(Ce)} building block.[19b] The $\{Ce_{10}\}$ cluster is captured by three dilacunary $\{P_2W_{16}\}$ building blocks, where every face-sharing $\{Ce_2\}$ group from the $\{Ce_6(Ce)\}$ hexagon is insetted in the vacancy of the dilacunary $\{P_2W_{16}\}$ units. The tridentate CO_3^{2-} structure-directing ligand is templated as the formation of the $\{Ce_3\}$ triangle, which is very uncommon in the $\{Ln_3\}$ sandwiched POM system.[28] Notably, the presence of the tridentate CO_3^{2-} ligand in **1a** has been confirmed by infrared spectroscopy showing an apparent band associated with the CO_3^{2-} ion (Figure S2).

Bond valence sum (BVS) calculations indicate that the seven Ce centers with +IV oxidation state are located on $\{Ce_6(Ce)\}$ hexagon (Ce1−Ce4), while the remaining Ce centers are +III (Ce5−Ce7) (Table S1). Six μ_2−OH bridges (O95, O97, O99, O100, O99A, O100A; BVS: −0.95 to −1.00) and 11 coordination water molecules (BVS: −0.29 to −0.38) in the $\{Ce_{10}\}$ cluster are also determined by the BVS calculations (Figure 2, Tables S2 and S3).[29] Notably, seven crystallographically independent Ce ions in **1** show four different coordination numbers and geometries: Ce(1,2,3) ions are all eight-coordinated and display the distorted square antiprisms, the seven-coordinated Ce(4) ion adopts the distorted monocapped trigonal prism, the ten-coordinated Ce(5) ion is embdedded in the distorted bicapped quadrangular prism, and the nine-coordinated Ce(6,7) ions reside in the distorted monocapped quadrangular antiprisms (Table S1). The involving Ce−O distances of 2.151(15)−2.729(14) Å for the Ce(IV) ions and 2.485(16)−2.610(33) Å for the Ce(III) ions fall in the usual ranges in related Ce(III) and Ce(IV) coordination complexes.[19b] The flexible coordination modes along with the diverse coordination numbers (from 7 to 10) of Ce(III) and Ce(IV) potentially provide them with a great likehood for creating more diverse high-nuclear Ce-based cluster embedded-POM architectures. From an architectural point of view, the hexagonal building units as well as pentagonal building blocks (such as $\{Mo_5(Mo)\}$) have partially spherical surfaces, which are indispensable components for building larger spherical clusters or curved frameworks. This motif has been observed in the field of Nd- and Gd-based Keplerates,[30] and Ce- and U-based clusters,[19b,31] which may potentially be important for the formation of larger spherical Ln-cluster embedded POMs.

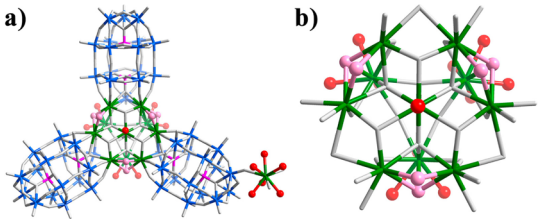

Figure 2. Structures of **1** (a) and $\{Ce_{10}\}$ cluster (b) with BVS assignments (W; blue sticks, Ce; green sticks, scheme outlined in Table S3).

Another interesting feature of **1** is that a 2D CBF (Figure 3a) is constructed by $\{Ce_{10}\}$ cluster embedded POT trimers **1a** and $[Ce^{III}(H_2O)_6]^{3+}$ bridges. In this framework, three **1a** trimers are joined together by one $[Ce^{III}(H_2O)_6]^{3+}$ cation, synchronously, every **1a** links to three $[Ce^{III}(H_2O)_6]^{3+}$ cations through Ce−O−W linkages. This structure can also be considered that three

DOI: 10.1021/acs.inorgchem.5b02473
Inorg. Chem. 2016, 55, 918−924

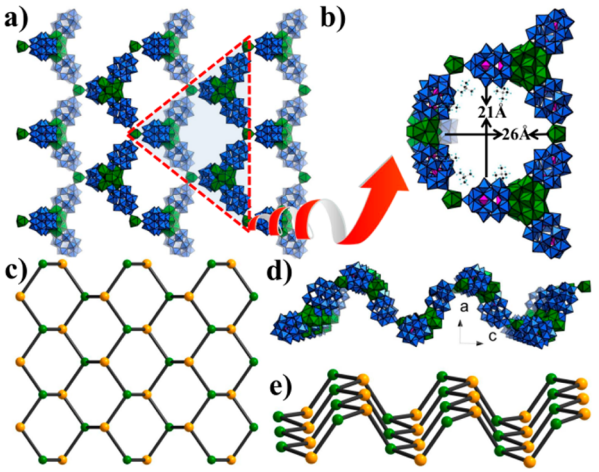

Figure 3. (a) The 2D framework of **1** along the *bc* plane with (b) the large cavity enclosed by three **1a** and three Ce^{III} ions; (c) the 2D graphite-like topology, the green and yellow balls represent the $\{Ce_{10}\}$ clusters and discrete Ce^{3+} ions, respectively, and the black rods represent the $\{P_2W_{16}\}$ linkers; (d) the 2D wave layer-like framework; and (e) the 2D graphite-like topology in the chair configuration of **1** down the *b* axis.

$\{Ce_{10}\}$ clusters and three discrere Ce^{3+} ions are connected by three $\{P_2W_{16}\}$ linkers alternately, generating a twisted chair-shaped six-member ring pore with the approximate size of 21 × 26 Å (Figure 3b). By this fashion, the 2D corrugated graphite-like topology framework is formed (Figure 3c–e), which is first encountered in CBF chemistry. More interestingly, two close layers are staggered and catenated with each other, forming a double-layer interpenetrating arrangement (Figure 4). These double layers are further stacked parallelly down the *b* axis, giving an organized array with the −A−B−A−B− pattern, in

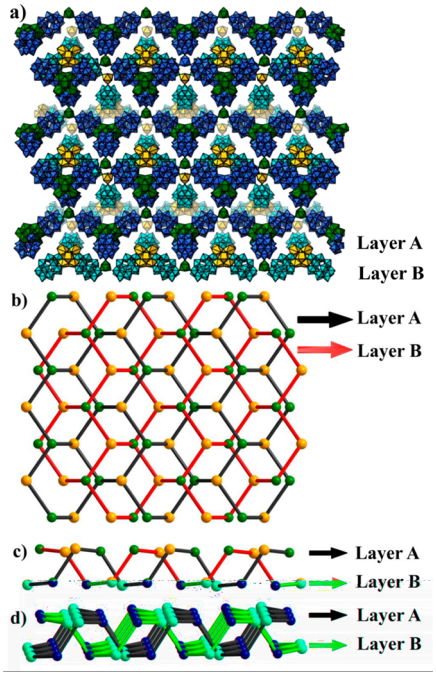

Figure 4. (a) The 2D wave layers are interconnected with each other viewed from *a* axis; the topological graph of the double-layer interpenetrating arrangement viewed down the (b) *a* axis and (c) *b* axis. (d) The view of the 2D wave interpenetrating layers.

which channels are filled with TMA cations and lattice water molecules accompanying abundant hydrogen bonding (Figure S3).

^{31}P Nuclear Magnetic Resonance. The behavior of **1** in solution was investigated by ^{31}P NMR (161.9 MHz, D_2O). The NMR spectrum of **1** exhibits two resonances located at −6.23 and −14.43 ppm with almost the same intensity (Figure 5a), in

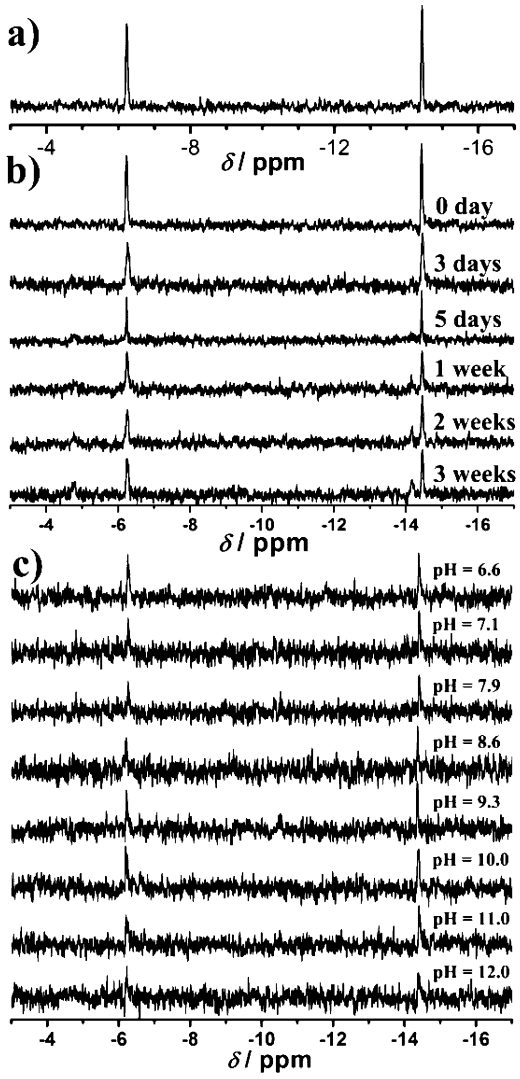

Figure 5. (a) ^{31}P NMR spectrum of **1** dissolved in D_2O at room temperature. (b) Evolution of the ^{31}P NMR spectra of **1** with time in D_2O. (c) Variable pH ^{31}P NMR spectra of **1** in D_2O/H_2O mixed solution.

which the downfield resonance is assigned to the phosphorus on the verge of the lacunary site of Dawson units, whereas the upfield resonance is assigned to the phosphorus in the other end of Dawson units. Two different sets of peaks in the NMR spectrum clearly indicate the presence of two kinds of P atoms in Dawson units, which is well consistent with the solid-state structure of **1** containing two types of P atoms. A survey of the ^{31}P NMR spectra for some lacunary Dawson-derived POTs indicates that the chemical shift of the phosphorus atom in the saturated site of Dawson units is steady, whereas the chemical shift of the phosphorus atom in the lacunary site of Dawson units is sensitive to the number of lacunary sites or the number and type of the atoms or groups encapsulated lacunary sites

DOI: 10.1021/acs.inorgchem.5b02473
Inorg. Chem. 2016, 55, 918–924

Table 2. ^{31}P NMR Chemical Shifts for Some Lacuary Dawson POMs

polyanion	chemical shifts	ref
$[\alpha_2\text{-}P_2W_{17}O_{61}]^{10-}$	−6.7, −14.1	20
$[\alpha\text{-}P_2W_{15}O_{56}]^{12-}$	+0.1, −13.3	20
$[\alpha\text{-}P_2W_{15}V_3O_{62}]^{9-}$	−6.8, −14.4	20
$\{[\alpha\text{-}P_2W_{15}O_{55}(H_2O)]Zr_3(\mu_3\text{-}O)(H_2O)(\text{L-tartH})[\alpha\text{-}P_2W_{16}O_{59}]\}^{15-}$	−6.29, −6.62, −12.88, −13.83	24a
$[(\alpha\text{-}P_2W_{16}O_{59})Zr_2(\mu_3\text{-}O)(C_4O_5H_3)]_2^{18-}$	−6.36, −6.46, −13.86, −13.87	24b
$[Zr_4(P_2W_{16}O_{59})_2(\mu_3\text{-}O)_2(\mu_2\text{-}OH)_2(H_2O)_4]^{14-}$	−6.45, −13.8	25
1a	−6.23, −14.43	this work

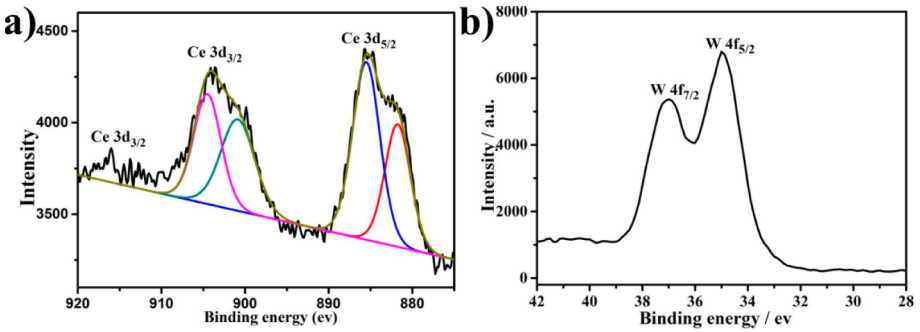

Figure 6. XPS spectra of (a) Ce 3d and (b) W 4f in **1**. The smooth line is a fitting of the spectral peaks. The two separate features ($3d_{3/2}$, higher binding energy feature; $3d_{5/2}$, lower binding energy feature) are due to spin−orbital splitting of the 3d core level.

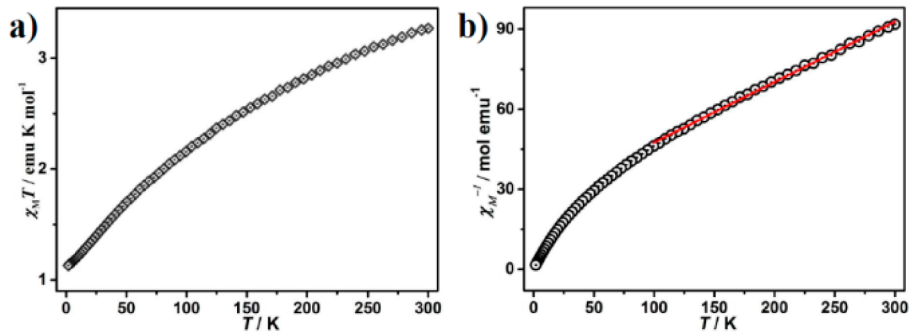

Figure 7. Temperature dependency of (a) $\chi_M T$ and (b) $1/\chi_M$ in the range of 1.8−300 K in 1000 Oe for **1**. Red solid line corresponds to the best fit (see text).

(Table 2). In addition, **1** can be stable and does not decompose over no less than 5 d; unexpectedly, a resonance of unknown species at −14.15 ppm began to appear after one week, which may be attributed to the α-$[P_2W_{17}O_{61}]^{10-}$ component derived from the part dissociation of **1**,[20] but the main NMR resonances of **1** still mainly exist (Figure 5b).

To study the pH-dependent stability of **1** in solution, pH-varied ^{31}P NMR spectra were also measured in aqueous solutions with different pH values (Figure 5c). The ^{31}P NMR spectrum in the unadjusted sample (pH 6.6) shows two signals were observed, and these signals maintained up to alkaline pH valus of 12.0. However, the intensity gradually decays along with the higher degree of alkali (especially above pH 10.0), maybe due to the solution becoming cloudy. In contrast, no signals were observed adjusting toward acid pH environment, resulting from the phosphorus constituents in **1** were almost completely precipitated below pH 6.0. Therefore, this compound was the predominant species within a wide pH range from 6.6 to 12.0 in base solution.

X-ray Photoelectron Spectroscopy. The XPS investigations on **1** were performed to confirm the valence states of Ce and W. The XPS spectra of Ce centers: the peaks around 904.4 and 885.5 eV in the energy regions of Ce $3d_{3/2}$ and Ce $3d_{5/2}$ correspond to Ce^{3+} ions;[32] whereas the characteristic XPS ($3d_{3/2}$) peak at 916.0 eV correspond to a transition from the initial state $3d^{10}4f^0$ to the final state $3d^94f^0$ of Ce^{4+} ions (Figure 6a).[33] The XPS spectra of W centers: the peaks around 37.1 and 35.0 eV in the energy regions of W $4f_{5/2}$ and W $4f_{7/2}$ are confirmed to be W^{6+} centers represented in Figure 6b.[34] This is consistent with BVS results.

Magnetic Property. Variable-temperature magnetic susceptibilities for **1** were measured in the temperature range of 1.8−300 K with an applied magnetic field of 1 kOe (Figure 7). The room-temperature $\chi_M T$ value is 3.26 emu K mol^{-1}, which is well close to the expected value of 3.21 emu K mol^{-1} (g = 6/7, J = 5/2) for four isolated Ce^{3+} ions in the $^2F_{5/2}$ ground state. On lowering of the temperature, the $\chi_M T$ product of **1** decreases gradually to a minimum of 1.13 emu K mol^{-1} at 1.8 K. Curve fitting for $1/\chi_M$ versus T plots of **1** with Curie−Weiss

DOI: 10.1021/acs.inorgchem.5b02473
Inorg. Chem. 2016, 55, 918−924

law in the range of 100−300 K results in C = 4.42 emu cm^3 K mol^{-1} and θ = −109.86 K. These results indicate that four Ce^{3+} ions reside in this formula and display anti-ferromagnetic interactions, which is consistent with the BVS results.

Proton Conductivity. Proton-conducting materials are an important component of fuel cells, which appears to be an attractive alternative energy converting system for the utilization of the alternative energy sources.[35] Recently, the newly developed proton-conducting materials have drawn great attention, which are mainly modularly built porous solids including coordination polymers, MOFs, or POM-MOFs. Generally, these materials require proton carriers given by acidic and/or hydrophilic groups and efficient proton transfer pathways composed of hydrophilic nono-channels or hydrogen-bond networks. In this field, MOFs act as new proton-conducting materials has been in vogue in recent years.[36] However, the proton-conducting studies about POMs materials are still in its infancy. Nevertheless, POMs solids possess abundant surface oxygen atoms, nano sizes, strong Brønsted acidity, and "pseudoliquid phase" behavior, which have been regarded as attractive candidates in designing new proton-conducting materials. Hence, loading POMs into the ordered channels of MOFs or directly assembling into CBFs would provide more hopping sites in the cavities and improve the stability and hydrophilicity of proton-conducting materials.[37,38] Therefore, the proton conductivity of **1** was investigated.

The proton conductivity of **1** was measured by AC impedance spectroscopy on pellet samples from 30 to 100 °C under 98% relative humidity (RH), and which was determined and evaluated from the semicircles in the Nyquist plots (Figure S4). The proton conductivity rapidly increases from 1.95 × 10^{-7} S cm^{-1} at 30 °C to 2.65 × 10^{-4} S cm^{-1} at 100 °C with 98% RH, which is indicative of the conductivity quickly increased with increasing temperature. This is slightly superior to the recently reported result of the POM-functionalized MOFs materials.[37] The temperature dependence of the proton conductivity was also measured for the bulk phase under 98% RH conditions (Figure 8a). The Arrhenius plot is approx-

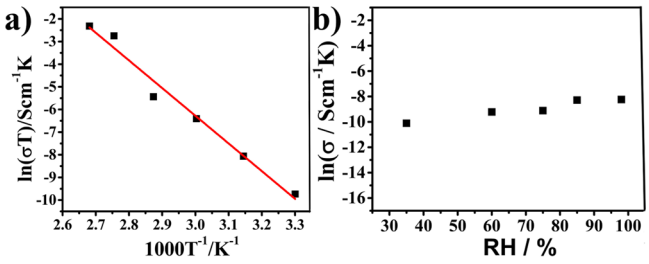

Figure 8. (a) Arrhenius plots of the proton conductivities of **1**. (b) log σ (S cm^{-1}) vs RH plots of **1** at 100 °C.

imately linear, affording that the activation energy (E_a) of the ionic conductivity is 0.36 eV. This value is very low enough to confirm that the conduction mechanism is the Grotthuss mechanism due to the activation energy in the range of 0.1−0.4 eV.[39] The result is reasonable because **1** contains lots of OH groups and water molecules with suitable hydrogen bond range of 2.69−2.82 Å. Protons hopping along the ordered hydrogen-bonded networks in 2D interlayers as protons conducting pathway contribute to the conductivity at the enhanced humidity.[39] This mechanism is obviously different from these reported MOF/POM systems usually observed for a vehicular mechanism (E_a > 0.6 eV),[38] whereas similar as the pure heteropolyacids systems (0.25−0.4 eV).[38a,40] In addition, the conductivity at 100 °C does hardly change with RH (Figure 8b and Figure S5), which can show good conductive characteristics that are less sensitive to surrounding conditions.

CONCLUDING REMARKS

In conclusion, we have successfully constructed an unprecedented 2D graphite-like CBF based on POTs units with {Ce_{10}} clusters and discrete Ce^{3+} ions. Moreover, the stability in aqueous solution and the pH-dependent stability are characterized by NMR. Its proton conductivity is probed here, which is first study on HLCIP-based CBF materials. From the viewpoint of preparative chemistry, these findings indicate that large HLCIP units (herein **1a**) can be used as CBUs to construct CBFs by means of coordination-driven effect of Ln connectors. More importantly, this research provides a possible methodology for constructing novel HLCIP-based CBF materials by selecting appropriate lacunary POM precursors and Ln cations. In the following time, this concept will be expanded to prepare much larger HLCIP units to create functional CBF materials with supralarge pores or channels. We will perform the catalysis and adsoption performaces of the HLCIP-based CBF materials.

ASSOCIATED CONTENT

Supporting Information

The Supporting Information is available free of charge on the ACS Publications website at DOI: 10.1021/acs.inorgchem.5b02473.

The schematic presentation of {P_2W_{16}}-based units, the additional structural figures of {Ce_{10}} cluster, IR spectra of **1**, BVS calculations, additional 2D graphite-like topological network of **1**, the equivalent circuit and Nyquist plots, TGA, PXRD, and EDX-SEM figures and related discussions. (PDF)

AUTHOR INFORMATION

Corresponding Authors

*E-mail: jyniu@henu.edu.cn. (J.N.)
*E-mail: jpwang@henu.edu.cn. (J.W.)

Notes

The authors declare no competing financial interest.

ACKNOWLEDGMENTS

We thank Dr. Z. Hao for his help during proton conductivity analysis. We gratefully acknowledge support from the NSFC and the Foundation of Education Department of Henan Province.

REFERENCES

(1) (a) Perry, J. J., IV; Perman, J. A.; Zaworotko, M. J. *Chem. Soc. Rev.* **2009**, *38*, 1400−1417. (b) Sava, D. F.; Kravtsov, V. C.; Eckert, J.; Eubank, J. F.; Nouar, F.; Eddaoudi, M. *J. Am. Chem. Soc.* **2009**, *131*, 10394−10396. (c) Han, Q.; He, C.; Zhao, M.; Qi, B.; Niu, J.; Duan, C. *J. Am. Chem. Soc.* **2013**, *135*, 10186−10189. (d) Furukawa, H.; Cordova, K. E.; O'Keeffe, M.; Yaghi, O. M. *Science* **2013**, *341*, 1230444.

(2) (a) Sarma, D.; Mahata, P.; Natarajan, S.; Panissod, P.; Rogez, G.; Drillon, M. *Inorg. Chem.* **2012**, *51*, 4495−4501. (b) Li, D.-S.; Zhao, J.; Wu, Y.-P.; Liu, B.; Bai, L.; Zou, K.; Du, M. *Inorg. Chem.* **2013**, *52*, 8091−8098.

DOI: 10.1021/acs.inorgchem.5b02473
Inorg. Chem. 2016, 55, 918−924

(3) (a) Oms, O.; Dolbecq, A.; Mialane, P. *Chem. Soc. Rev.* **2012**, *41*, 7497−7536. (b) Miras, H. N.; Yan, J.; Long, D.-L.; Cronin, L. *Chem. Soc. Rev.* **2012**, *41*, 7403−7430. (c) Kortz, U.; Müller, A.; van Slageren, J.; Schnack, J.; Dalal, N. S.; Dressel, M. *Coord. Chem. Rev.* **2009**, *253*, 2315−2327. (d) Zheng, S.-T.; Yang, G.-Y. *Chem. Soc. Rev.* **2012**, *41*, 7623−7646. (e) Coronado, E.; Giménez-Saiz, C.; Gómez-García, C. J. *Coord. Chem. Rev.* **2005**, *249*, 1776−1796. (f) Bo, Q. B.; Zhang, H. T.; Wang, H. Y.; Miao, J. L.; Zhang, Z. W. *Chem. - Eur. J.* **2014**, *20*, 3712−3723. (g) Hill, C. L. *J. Mol. Catal. A: Chem.* **2007**, *262*, 2−6. (h) Geletii, Y. V.; Botar, B.; Kögerler, P.; Hillesheim, D. A.; Musaev, D. G.; Hill, C. L. *Angew. Chem., Int. Ed.* **2008**, *47*, 3896−3899. (i) Han, X. B.; Zhang, Z. M.; Zhang, T.; Li, Y. G.; Lin, W.; You, W.; Su, Z. M.; Wang, E. B. *J. Am. Chem. Soc.* **2014**, *136*, 5359−5366. (j) Yin, Q.; Tan, J. M.; Besson, C.; Geletii, Y. V.; Musaev, D. G.; Kuznetsov, A. E.; Luo, Z.; Hardcastle, K. I.; Hill, C. L. *Science* **2010**, *328*, 342−345.

(4) (a) Zhao, J.-W.; Li, B.; Zheng, S.-T.; Yang, G.-Y. *Cryst. Growth Des.* **2007**, *7*, 2658−2664. (b) Yao, S.; Yan, J.-H.; Duan, H.; Zhang, Z.-M.; Li, Y.-G.; Han, X.-B.; Shen, J.-Q.; Fu, H.; Wang, E.-B. *Eur. J. Inorg. Chem.* **2013**, *2013*, 4770−4774. (c) Yao, S.; Zhang, Z.; Li, Y.; Wang, E. *Dalton Trans.* **2009**, 1786−1791.

(5) (a) Dolbecq, A.; Dumas, E.; Mayer, C. R.; Mialane, P. *Chem. Rev.* **2010**, *110*, 6009−6048. (b) Du, D.-Y.; Qin, J.-S.; Li, S.-L.; Su, Z.-M.; Lan, Y.-Q. *Chem. Soc. Rev.* **2014**, *43*, 4615−4632.

(6) Bassil, B. S.; Ibrahim, M.; Al-Oweini, R.; Asano, M.; Wang, Z.; van Tol, J.; Dalal, N. S.; Choi, K. Y.; Ngo Biboum, R.; Keita, B.; Nadjo, L.; Kortz, U. *Angew. Chem., Int. Ed.* **2011**, *50*, 5961−5964.

(7) Mal, S. S.; Kortz, U. *Angew. Chem., Int. Ed.* **2005**, *44*, 3777−3780.

(8) Godin, B.; Chen, Y. G.; Vaissermann, J.; Ruhlmann, L.; Verdaguer, M.; Gouzerh, P. *Angew. Chem., Int. Ed.* **2005**, *44*, 3072−3075.

(9) Zheng, S. T.; Zhang, J.; Clemente-Juan, J. M.; Yuan, D. Q.; Yang, G. Y. *Angew. Chem., Int. Ed.* **2009**, *48*, 7176−7179.

(10) Huang, L.; Wang, S. S.; Zhao, J. W.; Cheng, L.; Yang, G. Y. *J. Am. Chem. Soc.* **2014**, *136*, 7637−7642.

(11) Bassil, B. S.; Dickman, M. H.; Römer, I.; von der Kammer, B.; Kortz, U. *Angew. Chem., Int. Ed.* **2007**, *46*, 5985−5985.

(12) Wassermann, K.; Dickman, M. H.; Pope, M. T. *Angew. Chem., Int. Ed. Engl.* **1997**, *36*, 1445−1448.

(13) Hussain, F.; Spingler, B.; Conrad, F.; Speldrich, M.; Kogerler, P.; Boskovic, C.; Patzke, G. R. *Dalton Trans.* **2009**, 4423−4425.

(14) Hussain, F.; Patzke, G. R. *CrystEngComm* **2011**, *13*, 530−536.

(15) Hussain, F.; Conrad, F.; Patzke, G. R. *Angew. Chem., Int. Ed.* **2009**, *48*, 9088−9091.

(16) Hussain, F.; Gable, R. W.; Speldrich, M.; Kogerler, P.; Boskovic, C. *Chem. Commun.* **2009**, 328−330.

(17) Ritchie, C.; Moore, E. G.; Speldrich, M.; Kogerler, P.; Boskovic, C. *Angew. Chem., Int. Ed.* **2010**, *49*, 7702−7705.

(18) Fang, X.; Anderson, T. M.; Benelli, C.; Hill, C. L. *Chem. - Eur. J.* **2005**, *11*, 712−718.

(19) (a) Das, R.; Sarma, R.; Baruah, J. B. *Inorg. Chem. Commun.* **2010**, *13*, 793−795. (b) Malaestean, I. L.; Ellern, A.; Baca, S.; Kogerler, P. *Chem. Commun.* **2012**, *48*, 1499−1501.

(20) Contant, R. *Inorganic Syntheses* **1990**, *27*, 104−111.

(21) *SAINT, Program for Data Extraction and Reduction;* Bruker AXS, Inc: Madison, WI, 2001.

(22) Sheldrick, G. M. *SADABS—Bruker AXS area detector scaling and absorption,* version 2008/2001; University of Göttingen: Germany, 2008.

(23) Sheldrick, G. M. *Acta Crystallogr., Sect. A: Found. Crystallogr.* **2008**, *64*, 112−122.

(24) (a) Fang, X.; Anderson, T. M.; Hill, C. L. *Angew. Chem., Int. Ed.* **2005**, *44*, 3540−3544. (b) Fang, X.; Anderson, T. M.; Hou, Y.; Hill, C. L. *Chem. Commun.* **2005**, 5044−5046.

(25) Gaunt, A. J.; May, I.; Collison, D.; Travis Holman, K.; Pope, M. T. *J. Mol. Struct.* **2003**, *656*, 101−106.

(26) (a) Li, Y.-W.; Li, Y.-G.; Wang, Y.-H.; Feng, X.-J.; Lu, Y.; Wang, E.-B. *Inorg. Chem.* **2009**, *48*, 6452−6458. (b) Boyd, T.; Mitchell, S. G.; Miras, H. N.; Long, D.-L.; Cronin, L. *Dalton Trans.* **2010**, *39*, 6460−6465.

(27) Wang, X.; Chang, Z.; Lin, H.; Tian, A.; Liu, G.; Zhang, J. *Dalton Trans.* **2014**, *43*, 12272−12278.

(28) (a) Fang, X.; Anderson, T. M.; Neiwert, W. A.; Hill, C. L. *Inorg. Chem.* **2003**, *42*, 8600−8602. (b) Khoshnavazi, R.; Nicolò, F.; Amiri Rudbari, H.; Naseri, E.; Aminipour, A. *J. Coord. Chem.* **2013**, *66*, 1374−1383.

(29) (a) Brown, I. D.; Altermatt, D. *Acta Crystallogr., Sect. B: Struct. Sci.* **1985**, *41B*, 244−247. (b) Brese, N. E.; O'Keeffe, M. *Acta Crystallogr., Sect. B: Struct. Sci.* **1991**, *B47*, 192−197.

(30) Peng, J.-B.; Kong, X.-J.; Zhang, Q.-C.; Orendáč, M.; Prokleška, J.; Ren, Y.-P.; Long, L.-S.; Zheng, Z.; Zheng, L.-S. *J. Am. Chem. Soc.* **2014**, *136*, 17938−17941.

(31) Ling, J.; Wallace, C. M.; Szymanowski, J. E. S.; Burns, P. C. *Angew. Chem., Int. Ed.* **2010**, *49*, 7271−7273.

(32) (a) Ding, J.; Weng, L.-T.; Yang, S. *J. Phys. Chem.* **1996**, *100*, 11120−11121. (b) Chen, W.-C.; Qin, C.; Wang, X.-L.; Li, Y.-G.; Zang, H.-Y.; Shao, K.-Z.; Su, Z.-M.; Wang, E.-B. *Dalton Trans.* **2015**, *44*, 11290−11293.

(33) (a) Fujimori, A. *Phys. Rev. B: Condens. Matter Mater. Phys.* **1983**, *28*, 2281−2283. (b) Kim, D. K.; Stöwe, K.; Müller, F.; Maier, W. F. *J. Catal.* **2007**, *247*, 101−111. (c) Kim, J.-H.; Tsuchiya, B.; Nagata, S.; Shikama, T. *Solid State Ionics* **2008**, *179*, 1182−1186.

(34) Chen, W.-C.; Wang, X.-L.; Jiao, Y.-Q.; Huang, P.; Zhou, E.-L.; Su, Z.-M.; Shao, K.-Z. *Inorg. Chem.* **2014**, *53*, 9486−9497.

(35) Yoon, M.; Suh, K.; Natarajan, S.; Kim, K. *Angew. Chem., Int. Ed.* **2013**, *52*, 2688−2700.

(36) (a) Xu, G.; Otsubo, K.; Yamada, T.; Sakaida, S.; Kitagawa, H. *J. Am. Chem. Soc.* **2013**, *135*, 7438−7441. (b) Bhattacharya, S.; Bhattacharyya, A. J.; Natarajan, S. *Inorg. Chem.* **2015**, *54*, 1254−1271.

(37) Liu, Y.; Yang, X.; Miao, J.; Tang, Q.; Liu, S.; Shi, Z.; Liu, S. *Chem. Commun.* **2014**, *50*, 10023−10026.

(38) (a) Wei, M.; Wang, X.; Duan, X. *Chem. - Eur. J.* **2013**, *19*, 1607−1616. (b) Yang, L.; Ma, P.; Zhou, Z.; Wang, J.; Niu, J. *Inorg. Chem.* **2013**, *52*, 8285−8287. (c) Wei, M.-L.; Zhuang, P.-F.; Li, H.-H.; Yang, Y.-H. *Eur. J. Inorg. Chem.* **2011**, *2011*, 1473−1478.

(39) (a) Colomban, P.; Novak, A. *J. Mol. Struct.* **1988**, *177*, 277−308. (b) Taylor, J. M.; Mah, R. K.; Moudrakovski, I. L.; Ratcliffe, C. I.; Vaidhyanathan, R.; Shimizu, G. K. H. *J. Am. Chem. Soc.* **2010**, *132*, 14055−14057.

(40) (a) Kreuer, K. D.; Hampele, M.; Dolde, K.; Rabenau, A. *Solid State Ionics* **1988**, *28*−*30*, 589−593. (b) Misono, M. *Chem. Commun.* **2001**, 1141−1152.

DOI: 10.1021/acs.inorgchem.5b02473
Inorg. Chem. 2016, 55, 918−924